

THE EFFECT OF POROSITY ON X-RAY EMISSION LINE PROFILES FROM HOT-STAR WINDS

STANLEY P. OWOCKI¹ AND DAVID H. COHEN²

¹Bartol Research Institute, Department of Physics & Astronomy, University of Delaware, Newark, DE 19716
and

²Department of Physics, Swarthmore College, Swarthmore, PA 19081

Draft version January 18, 2006

ABSTRACT

We investigate the degree to which the nearly symmetric form of X-ray emission lines seen in Chandra spectra of early-type supergiant stars can be explained by the porous nature of their spatially structured stellar winds. Such porosity could effectively reduce the bound-free absorption of X-rays emitted by embedded wind shocks, and thus allow a more similar transmission of red- vs. blue-shifted emission from the back vs. front hemispheres. For the localized self-shielding that is central to the porosity effect, it is necessary that the individual clumps be optically thick, which, for a given opacity and mean density, depends on the ratio of the clump scale ℓ to its volume filling factor f . For a simple parameterization in which this ‘porosity length’ $h \equiv \ell/f$ increases with local radius r as $h = h' r$, we find that a substantial reduction in wind absorption requires a quite large porosity length gradient, $h' \gtrsim 1$, implying large porosity lengths $h \approx r$. The associated wind structure must thus either have either a relatively large scale $\ell \lesssim r$, or a small volume filling factor $f \approx \ell/r \ll 1$, or some combination of these. We argue that the relatively small-scale, moderate compressions generated by intrinsic instabilities in line-driving are unlikely to give such large porosity lengths. This raises questions about whether porosity effects could play a significant role in explaining nearly symmetric X-ray line profiles, leaving again the prospect of instead having to invoke a substantial (ca. factor 5) downward revision in the assumed mass loss rates.

Subject headings: line: profiles — stars: early-type — stars: mass loss — stars: winds, outflow — X-rays: stars

1. INTRODUCTION

The high sensitivity and high spectral resolution of spectrometers on the Chandra X-ray observatory have made it possible to resolve X-ray emission line profiles from several hot, bright supergiant stars, e.g. ζ Pup and ζ Ori. The general broadness of these emission lines, with velocity half-widths of ca. 1000 km/s, is generally consistent with the idea that the X-rays are emitted in the expanding, highly supersonic stellar wind, perhaps from embedded shocks generated by instabilities associated with the line-driving of the overall wind outflow. However, these profiles are also generally quite symmetric between the red and blue side, implying a relative small degree of attenuation of the red side emission thought to originate in the back hemisphere relative to the observer.

In the standard wind-shock picture, the X-ray emitting gas is expected to only occupy a small fraction ($< 1\%$) of the volume, with the bulk of the wind consisting of relatively cool material with a substantial X-ray opacity from bound-free transitions of He and heavier ions. For expected mass loss rates for these stars, the bound-free optical depths along a radial ray to the surface are expected to be of order $\tau_* \approx 10$. Since this implies a substantial attenuation of red-shifted emission originating from the back hemisphere, the expected X-ray emission line profiles have a marked asymmetric form, with a much stronger blue side and lower, more attenuated red side. Within a simple parameterized model, fitting the more symmetric observed profiles has required a substantial (factor 5!) reduction in the assumed wind mass loss

rates. If substantiated, such a radical reduction in supergiant mass loss would have far-reaching consequences for both massive star evolution and the broad influence of wind mass loss on the structure of the interstellar medium.

This paper investigates an alternative scenario in which the reduction in wind attenuation might instead result from a spatially *porous* nature of the stellar wind. If wind material is compressed into localized, optically thick clumps, then red-shifted emission from the back hemisphere might be more readily transmitted through the relatively low-density, channels or porous regions between the clumps. Feldmeier, Oskinova, & Hamman (2003) and Oskinova, Feldmeier, & Hamman (2004) have in fact examined such effects in quite detailed models that assume a specific ‘pancake’ form for the dense structures, under the presumption that these would arise naturally from the strong radial compressions associated with the intrinsic instability of the line-driving of such hot-star winds. Although 1D models of the nonlinear evolution do lead to compression into geometrically thin shells (Owocki, Castor, & Rybicki 1988; Feldmeier 1995), recent 2D models (Dessart & Owocki 2003, 2005) suggest the structure may instead break into clumps with a similarly small lateral and radial scale.

MORE ON WHY OUR PARAMETERIZED APPROACH HAS ITS ADVANTAGES FOR ILLUMINATING THE KEY PROPERTIES NEEDED TO MAKE POROSITY WORK

2. CLUMPING VS. POROSITY EFFECTS IN A STRUCTURED MEDIUM

2.1. Density-Square Clumping Correction

Before discussing how porosity effects can alter diagnostics like bound-free absorption that scale linearly with density, it is helpful first to review briefly the usual account of how the clumping of a medium can alter diagnostics that scale with the *square* of the density. For example, emission or absorption from atomic states that arise from recombination or collisional excitation depends on the proximate interaction of two constituents, e.g. electrons and ions, and thus scales with the product of their individual particle density, e.g. $n_e n_i$, which for a fixed ionization and abundance is simply proportional to the square of the mass density, ρ^2 . The effect of spatial structure on such diagnostics is thus traditionally accounted for in terms of a simple density-square clumping correction factor,

$$C_c \equiv \frac{\langle \rho^2 \rangle}{\langle \rho \rangle^2}, \quad (1)$$

where the angle brackets denote a volume averaging. For example, in a simple model in which clumps of scale ℓ and mass m_c are separated by a mean distance $L \gg \ell$, the mean density is $\langle \rho \rangle = m_c/L^3$, whereas the individual clump density $\rho_c = m_c/\ell^3 = \langle \rho \rangle (L/\ell)^3$. Application in eqn. (1) then implies that the clumping correction is just given by the inverse of the volume filling factor,

$$C_c = \frac{L^3}{\ell^3} \equiv \frac{1}{f}. \quad (2)$$

For diagnostics of wind mass loss rate, e.g. Balmer or radio emission, the associated reduction in inferred mass loss scales as $\dot{M} \sim \sqrt{C_c}$.

A key point here is that this density-squared clumping correction depends only the volume filling factor, $f = \ell^3/L^3$, and *not* on the scale ℓ of individual clumps. As long as the emission can escape from each local emitting clump, the correction factor thus applies to structure ranging, for example, from very small-scale instability-generated turbulence, to possible stellar-scale magnetically confined loops.

2.2. Porosity Reduction in Linear-Density Opacity for Optically Thick Clumps

The attenuation of X-rays emitted within a stellar wind occurs through bound-free absorption, primarily from the ground-state. Since this is the dominant stage of the absorbing ions, and exists independently of interaction with other particles, the associated absorption scales only *linearly* with density, with the volume opacity (attenuation per unit length) given by $\chi = \kappa\rho$, where the mass opacity (mass absorption coefficient) has units of a cross section per unit mass, e.g. cm^2/g in CGS.

If, however, we consider the above clump model in the case when the individual clumps are *optically thick*, then the “effective opacity” of the clump ensemble can be written in terms of the ratio of the physical cross section of the clumps to their mass,

$$\kappa_{eff}^{thick} = \frac{\ell^2}{m_c} = \frac{\kappa}{\tau_c} \quad ; \quad \tau_c \gg 1. \quad (3)$$

The latter equality shows that, relative to the atomic opacity κ , this effective opacity is reduced by a factor that scales with the inverse of the clump optical thickness, $\tau_c = \kappa\rho_c\ell = \kappa\langle\rho\rangle\ell/f$.

Note that the clump optical thickness that determines the effective opacity reduction depends on the *ratio* of the clump *scale* to the volume filling factor, a quantity which we shall call the “porosity length” $h \equiv \ell/f$. This represents an essential distinction between the porosity effect and the usual density-squared clumping correction, which as noted above depends only on the volume filling factor without dependence on the clump size scale.

The above scaling also serves to emphasize another key requirement for porosity, namely the *local self shielding* of material within optically thick clumps, allowing then for a more transparent transmission of radiation through the “porous” interclump channels.

3. GENERAL POROSITY LAW BRIDGING OPTICALLY THIN AND THICK CLUMP LIMITS

To generalize the above effective opacity to a scaling that applies to both the optically thick and thin limits, consider that the effective absorption of clumps is set by the geometric cross section times an absorption fraction, $\sigma_{eff} = \ell^2[1 - \exp(-\tau_c)]$. Applying this to modify the scaling in eqn. (3), we obtain a general porosity reduction in opacity of the form,

$$\frac{\kappa_{eff}}{\kappa} = \frac{1 - e^{-\tau_c}}{\tau_c}. \quad (4)$$

This gives the reduced opacity $\kappa_{eff}/\kappa \approx 1/\tau_c$ of eqn. (3) in the optically thick clump limit $\tau_c \gg 1$, but recovers the atomic opacity $\kappa_{eff} \approx \kappa$ in the optically thin limit $\tau_c \ll 1$.

An alternative bridging scaling can be derived by focussing on the effective mean path length within the medium, which scales with the inverse of the effective volume opacity, $1/\kappa_{eff}\langle\rho\rangle$. Within a model in which such an effective opacity adds in inverse of contributing components (much as Rosseland mean opacity defined for weighting frequency-averaged opacity), we add the microscopic and clump components of path length as,

$$\frac{1}{\kappa_{eff}\langle\rho\rangle} = \frac{1}{\kappa\langle\rho\rangle} + h, \quad (5)$$

where we note that the porosity length defined above also defines a mean free path between clumps, $h \equiv \ell/f = L^3/\ell^2$. This scaling solves to a general effective opacity scaling of the form

$$\frac{\kappa_{eff}}{\kappa} = \frac{1}{1 + \tau_c}. \quad (6)$$

This again gives both the correct forms in the opposite asymptotic limits of optically thin vs. thick clumps. For moderately small optical depths $\tau \lesssim 1$, Taylor expansion shows the reduction is somewhat steeper for the mean-path form of eqn. (6), i.e. as $1 - \tau_c$ instead of the slightly weaker $1 - \tau_c/2$ for the absorption scaling of eqn. (4). But the plot in fig. 1 shows that both forms have a very similar overall variation with clump optical depth.

4. POROSITY EFFECT ON WIND OPTICAL DEPTH

The above formalism provides a convenient way to explore the effect of porosity on wind attenuation of X-ray emission. Our basic approach here is to generalize the parameterized analysis of Owocki & Cohen (2001) (hereafter OC) to include the porosity reduction in effective

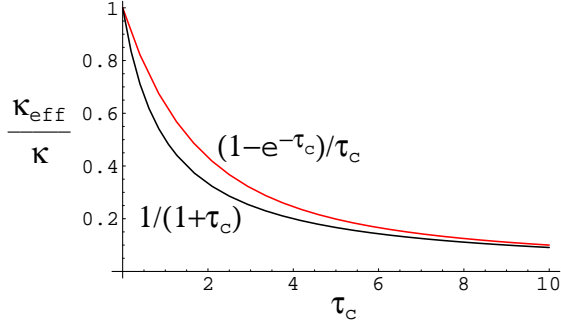


FIG. 1.— Comparison of absorption (upper curve) and mean-path (lower curve) scalings of effective opacity of porous medium, plotted as a function of clump optical thickness τ_c .

absorption. For effective opacity, we choose to work with the slightly simpler mean-path form (6), which avoids the complicating effects of the exponential function, with the clump optical thickness correction only appearing in a single term in the denominator. Following eqn. (OC-1), the effective optical depth to a position z along a ray with impact parameter p is now written as

$$t_{eff}[p, z] = \int_z^\infty \frac{\kappa \rho[r']}{1 + \kappa \rho[r'] h[r']} dz' \quad (7)$$

where $\rho[r']$ is now the smoothed out mass density at radius $r' \equiv \sqrt{p^2 + z'^2}$, and $h[r']$ is the (possibly radially dependent) porosity length. For a steady-state wind with a simple (“beta=1”) velocity law of the form $w(r) \equiv v(r)/v_\infty = (1 - R_*/r)$, this becomes [cf. eqn. (OC-4)],

$$t_{eff}[p, z] = \tau_* \int_z^\infty \frac{R_* dz'}{r'(r' - R_*) + \tau_* h[r']}, \quad (8)$$

where, as in Owocki & Cohen (2001), we have here used the mass loss rate, $\dot{M} \equiv 4\pi\rho v r^2$, to define a characteristic wind optical depth¹, $\tau_* \equiv \kappa \dot{M}/4\pi v_\infty R_*$. As in eqn. (OC-4), for rays intersecting the core ($p \leq R_*$), eqn. (8) is restricted to locations in front of the star, i.e. $z > \sqrt{R_*^2 - p^2}$, since otherwise the optical depth becomes infinite, due to absorption by the star.

For the physically quite reasonable case that the porosity length expands linearly with the radius, i.e. as $h = h' r$, the integral in eqn. (8) can be integrated analytically to give [cf. eqn. (OC-5)]

$$\frac{t_{eff}[p, z]}{\tau_*} = \left[\frac{\arctan\left(\frac{R_*(1 - \tau_* h') z'}{r' z_h}\right) + \arctan\left(\frac{z'}{z_h}\right)}{z_h} \right]_{z'=z}^{z' \rightarrow \infty}, \quad (9)$$

where $z_h \equiv \sqrt{p^2 - R_*^2(1 - \tau_* h')^2}$. Writing the direction cosine $\mu = z/r$, the effective optical depth as a function of spherical coordinates is given by

$$\tau_{eff}[\mu, r] = t \left[\sqrt{1 - \mu^2} r, \mu r \right]. \quad (10)$$

If we assume the local line emission in the wind has a narrow, delta-function line-profile, then at any given

¹ Note that in a smooth wind with a constant velocity $v = v_\infty$, the radial ($p = 0$) optical depth at radius r would be given simply by $t[0, r] = \tau_* R_*/r$. Thus in such a constant-velocity wind, τ_* would be the radial optical depth at the surface radius R_* , while $R_1 = \tau_* R_*$ would be the radius of unit radial optical depth.

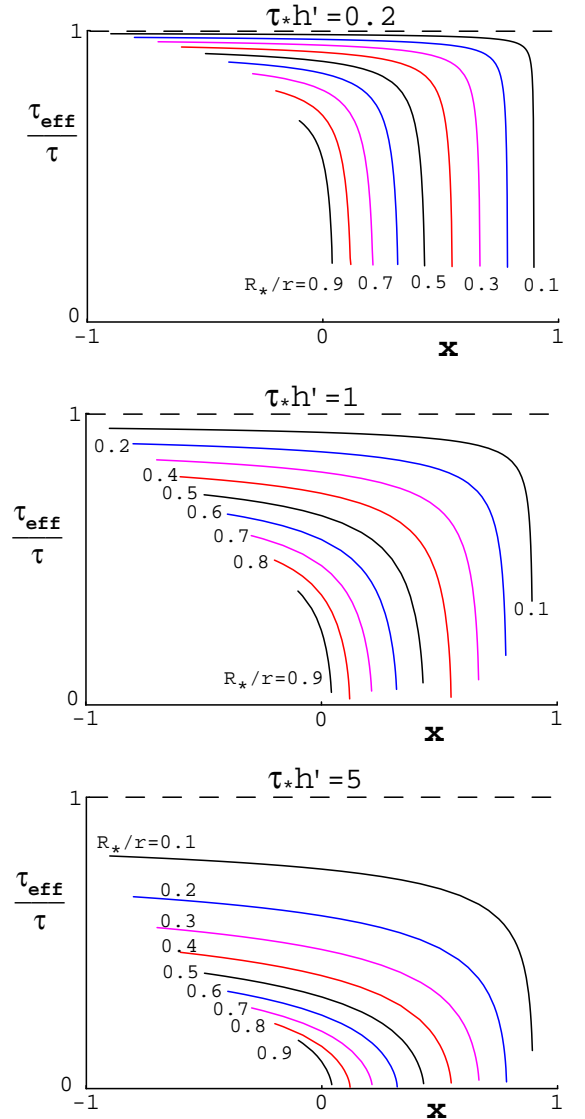


FIG. 2.— Ratio of the effective optical depth to optical depth in smooth wind, $\tau[-x/w(r), r]/\tau[-x/w(r), r]$, plotted vs. the scaled wavelength x , at selected radii r in porosity models with $\tau_* h' = 0.2, 1, \text{ and } 5$ (top to bottom).

radius the projected Doppler-shift from the wind velocity depends only on direction cosine μ . This leads to the simple transformation $\mu \rightarrow -x/w(r)$, where $w(r) = v(r)/v_\infty = 1 - R_*/r$ is the scaled velocity law, and $x \equiv (\lambda/\lambda_0 - 1)c/v_\infty$ is the Doppler shift in wavelength λ from line center λ_0 , measured in units of the wind terminal speed v_∞ .

Figure 2 plots the porosity reduction in optical depth vs. wavelength x , for a selection of source radii r , with the panels from top to bottom assuming increasing porosity parameterized by $\tau_* h' = 0.2, 1, \text{ and } 5$. In the top panel, the steep reductions are only near those frequencies that, for the given source radius, require ray passage through the very inner wind, where the high density makes the clumps optically thick even for the modest porosity gradient. Since this also generally means the overall optical depth in these regions is also quite high, the reductions still do not make the regions very transparent. For the increasing porosity cases in the middle and lower panels the reduction in optical depth occurs

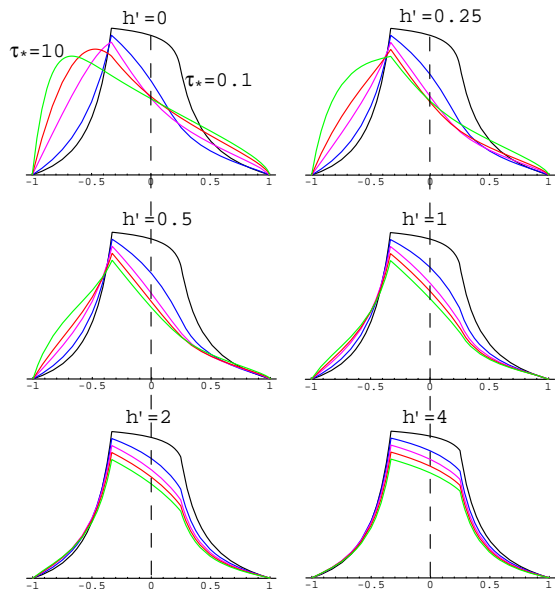


FIG. 3.— X-ray line profiles vs. scaled wavelength x , overplotted in each panel for optical depth parameters $\tau_* = 0.1, 1, 3, 5$, and 10 (black, blue, violet, red, green), normalized to have peaks decrease by 5% for each step in τ_* . The panels compare results for various porosity length gradients $h' = 0, 0.25, 0.5, 1, 2$, and 4, ordered from upper left to lower right.

over a much broader range of frequencies. These large porosity cases can thus indeed lead to a more transparent wind, with, as we now show, notable changes in the line profile.

5. POROSITY EFFECT ON X-RAY EMISSION LINE PROFILES

With the optical depths in hand, the computation of the emission line profiles follows directly the approach by Owocki & Cohen (2001). The wavelength-dependent X-ray luminosity can then be evaluated from a single integral in inverse radius $u \equiv R_*/r$ [cf. eqn. (OC-9)]

$$L_x \propto \int_0^{u_x} \frac{du}{(1-u)^3} e^{-\tau_{eff}[-x/(1-u), R_*/u]}, \quad (11)$$

REFERENCES

Cassinelli, J. P., Cohen, D. H., MacFarlane, J. J., Sanders, W. T., & Welsh, B. Y. 1994, *ApJ*, 421, 705
 Cassinelli, J. P., Miller, N. A., Waldron, W. L., MacFarlane, J. J., & Cohen, D. H. 2001, *ApJ*, 554, L55
 Cohen, D. H., Cooper, R. G., MacFarlane, J. J., Owocki, S. P., Cassinelli, J. P. & Wang, P. 1996, *ApJ*, 460, 506
 Cohen, D. H., de Messières, G. E., MacFarlane, J. J., Miller, N. A., Cassinelli, J. P., Owocki, S. P., & Liedahl, D. A. 2003, *ApJ*, 586, 495
 Cooper, R. G. 1996, Ph.D. thesis, University of Delaware
 Corcoran, M. F., et al. 1993, *ApJ*, 412, 792
 Dessart, L. & Owocki, S. P. 2003, *A&A*, 406, L1
 Dessart, L., & Owocki, S. P. 2005, *A&A*, 437, 657
 Feldmeier, A. 1995, *A&A*, 299, 523
 Feldmeier, A., Kudritzki, R.-P., Palsa, R., Pauldrach, A. W. A., & Puls, J. 1997, *A&A*, 320, 899
 Feldmeier, A., Oskinova, L., & Hamman, W.-R. 2003, *A&A*, 403, 217
 Feldmeier, A., Puls, J., & Pauldrach, A. W. A. 1997, *A&A*, 322, 878
 Fullerton, A. W., Massa, D. L., & Prinja, R. K. 2004, *BAAS*, 205, 5304
 Hillier, D. J., Kudritzki, R. P., Pauldrach, A. W., Baade, D., Cassinelli, J. P., Puls, J., & Schmitt, J. H. M. M. 1993, *ApJ*, 276, 117

where $u_x \equiv \min[R_*/R_o, 1 - |x|]$. For simplicity, we have assumed here that the X-ray volume filling factor is zero below a minimum X-ray emission radius R_o , and constant above this (i.e. the OC $q = 0$ case).

Fig. 3 compares line profiles for various porosity gradient values, from the no porosity case ($h' = 0$; upper left) to large gradient ($h' = 4$; lower right). Note that the profiles with large optical depth $\tau_* = 10$ (green curves, displaced to be the lowest in each panel) have strong blue-shift asymmetry for cases with no or moderate porosity, ($h' \leq 1$), and approach the near symmetry of the optically thin ($\tau_* = 0.1$; black curves, displaced to have highest peak) only for models with very large porosity length gradient, $h' = 2, 4$ (lowermost panels).

Thus the basic result here is that achieving a near symmetry in line-profiles for models with a large optical depth requires very large porosity lengths, $h > r$. Since $h \equiv \ell/f$, this requires that the wind structure have either a very large scale, $\ell \gtrsim r$, or a small filling factor, $f < \ell/r$, or some combination of these.

6. DISCUSSION

DISCUSSION OF GENERAL IMPLICATIONS OF LARGE POROSITY LENGTH REQUIREMENT FOR LIKELIHOOD THAT POROSITY COULD BE GENERAL EXPLANATION FOR SYMMETRIC PROFILES. SPECIFICALLY COMMENT ON DIFFICULTY OF GETTING SUCH LARGE POROSITY LENGTHS FROM LDI. EMPHASIZE ALSO THAT POROSITY MODEL HERE MORE LIKELY OVERESTIMATES A MORE REALISTIC MODEL, E.G. WITH DISTRIBUTION OF POROSITY LENGTHS.

7. SUMMARY

SUMMARIZE RESULTS; DISCUSS FUTURE WORK. EMPHASIZE IMPLICATIONS OF NEED TO LOWER MDOTS.

Ignace, R. 2001, *ApJ*, 549, L119
 Kramer, R. H., Cohen, D. H., & Owocki, S. P. 2003, *ApJ*, 592, 532
 Kramer, R. H., Tonnesen, S. K., Cohen, D. H., Owocki, S. P., ud-Doula, A., & MacFarlane, J. J. 2003, *Rev. Sci. Instr.*, 74, 1966
 Kudritzki, R. P., Palsa, R., Feldmeier, A., Puls, J. & Pauldrach, A. W. A. 1996, in *Röntgenstrahlung from the Universe*, eds. H. U. Zimmermann, J. Trümper, & H. Yorke (Munich: MPE), 9
 Leutenegger, M., Paerels, F., Kahn, S., & Cohen, D. H. 2006, in preparation
 Miller, N. A., Cassinelli, J. P., Waldron, W. L., MacFarlane, J. J., & Cohen, D. H. 2002, *ApJ*, 577, 951
 Oskinova, L., Feldmeier, A., & Hamman, W.-R. 2004, *A&A*, 422, 675
 Owocki, S. P., Castor, J. I., & Rybicki, G. B. 1988, *ApJ*, 335, 914
 Owocki, S. P., & Cohen, D. H. 1999, *ApJ*, 520, 833
 Owocki, S. P. & Cohen, D. H. 2001, *ApJ*, 559, 1108
 Owocki, S. P., Gayley, K. G. & Shaviv, N. J. 2004, *ApJ*, 616, 525
 Owocki, S. P. & Rybicki, G. B. 1984, *ApJ*, 284, 337
 Runacres, M. C. & Owocki, S. P. 2002, *A&A*, 381, 1015
 ud-Doula, A., & Owocki, S. P. 2002, *ApJ*, 576, 413
 Waldron, W. L. 1984, *ApJ*, 282, 256
 Waldron, W. L., & Cassinelli, J. P. 2001, *ApJ*, 548, L45